Catena 121 (2014) 68–80

Contents lists available at ScienceDirect

Catena

journal homepage: www.elsevier.com/locate/catena

The dust provenance and transport mechanism for the Chengdu Clay in the Sichuan Basin, China

Jin-Liang Feng *, Zhao-Guo Hu, Jian-Ting Ju, Yong-Chong Lin

Key Laboratory of Tibetan Environment Changes and Land Surface Processes, Institute of Tibetan Plateau Research, Chinese Academy of Sciences, Beijing 100101, China

ARTICLE INFO

Article history:
Received 12 April 2013
Received in revised form 10 March 2014
Accepted 29 April 2014
Available online xxxx

Keywords:
Loess
Chengdu Clay
Dust transport
Sichuan Basin
Tibetan Plateau
Chinese Loess Plateau

ABSTRACT

The Chengdu Clay in the Sichuan Basin, China, was named by Thorp and Dye in 1936. The genesis, dust provenance and transport mechanism for the Chengdu Clay, however, are still debated. In the present work, the Chengdu Clay and adjacent loess from the eastern Tibetan Plateau, the Chinese Loess Plateau and the Qinling Mountains were investigated. The content and grain size distribution of quartz, quartz $\delta^{18}O$, Sm–Nd isotopic system, rare earth elements and other trace element concentrations for the Chengdu Clay and its adjacent loess were analyzed. Based on comparison and spatial variation analysis, the results confirm that the Chengdu Clay is of aeolian origin. The dust provenance of the Chengdu Clay differs from those of the adjacent loess. The Chengdu Clay is possibly of local origin and is transported by an ancient katabatic wind over a short distance during glacial and stadial periods. The alluvial sediments in the northwestern Sichuan Basin are possibly the major sources of the Chengdu Clay. There is little possibility of an effective aeolian transport bringing dust from the Tibetan Plateau, the arid area in northwestern China or Inner Mongolia into the Sichuan Basin, where it may be deposited to form the Chengdu Clay. Thus, long-range dust transport by the East Asian winter monsoon, the westerly jet or the Tibetan Plateau winter monsoon possibly plays a minor role in controlling the magnitude of the dust flux of the Chengdu Clay in the Sichuan Basin.

1. Introduction

The Chengdu Clay (Chengtu Clay; CDCL) was named by Thorp and Dye in 1936. According to the description by Thorp and Dye (1936), the Chengdu Clay is characterized by the following properties: (1) distributed in the western and northwestern parts of the Sichuan Basin (Szechwan Basin), (2) near surface outcrop, (3) covering the second and higher terraces or rocky hills, (4) no stratification, (5) no columnar structure, (6) containing calcareous concretions, (7) no gravel or pebble, (8) moderately or slightly acid to neutral reaction, (9) yellow sticky and plastic clay, (10) weathered after deposition, (11) formed in the late Pleistocene, and (12) possible aeolian origin.

Thorp and Dye (1936), Salfeld (1936), and additional investigators (Chu, 1937; Thorp, 1939; Richardson, 1942, 1943; Ma, 1944; Liu, 1983; Shao et al., 1984; Fang, 1995; Feng et al., 2010, 2011; Hu et al., 2010; Yang et al., 2010a, b) confirm that CDCL is possibly a weathered aeolian deposit. In contrast, Young (1937) and other researchers express different opinions regarding the aeolian origin of CDCL (Yü, 1940; Hseung, 1944; Li, 1947; Li et al., 1964; Zhou, 1986; Zhang, 1988; Kong, 1994). Moreover, the original relationships among the CDCL, the loess of the eastern Tibetan Plateau (ETPL), the loess of the Chinese Loess Plateau and the Qinling Mountains (Tsinling Mountains; LPQL), and their potential source areas are still debated (Thorp and Dye, 1936; Thorp, 1939; Richardson, 1942, 1943; Ma, 1944; Lu et al., 1976; Shao et al., 1984; Fang, 1995; Wang, 1998; Wang et al., 2002; Feng et al., 2010, 2011; Hu et al., 2010; Yang et al., 2010a,b). Accordingly, the wind systems for dust transport in the Sichuan Basin are also a debated problem (Fang, 1995; Feng et al., 2010, 2011; Han et al., 2010; Hu et al., 2010; Yang et al., 2010a,b).

Aeolian deposits are very important for understanding soil genesis, aeolian dust aggradation, wind erosion, palaeoclimate, source-area aridity and plant cover (Rea, 1994; Derbyshire et al., 1998; Muhs and Bettis, 2000; Stuut et al., 2009; Maher et al., 2010). A large number of studies focusing on the aeolian deposits in Asia, particularly in China, have been reported so far (Liu and Chang, 1964; Heller and Liu, 1982; Liu, 1985; Kukla et al., 1988; Porter and An, 1995; Derbyshire et al., 1997), but the investigations on the aeolian sediments in the Sichuan Basin are relatively few (Zhao et al., 2007; Han et al., 2010; Yang et al., 2010b). In addition, the investigations of the aeolian sediments in the Sichuan Basin may shed light on whether or not the Tibetan Plateau is an important dust source for long-range transport in Asia (Clarke, 1995; Fang, 1995; Zhang et al., 1996, 2001; Lehmkuhl et al., 2000; Fang et al., 2004; Lu et al., 2004; Sun et al., 2007a; Han et al., 2008; Kapp et al., 2011).

The objectives of this study were to investigate (1) the original relationships between CDCL with adjacent loess (ETPL and LPQL); (2) the

* Corresponding author at: Institute of Tibetan Plateau Research, Chinese Academy of Sciences, Building 3, 16th Lincui Road, Chaoyang, Beijing 100101, China. Tel.: +86 10 84097095; fax: +86 10 84097079.
E-mail address: fengjl@itpcas.ac.cn (J.-L. Feng).

http://dx.doi.org/10.1016/j.catena.2014.04.018
0341-8162/

transport mechanism and potential source areas of the CDCL; and (3) the meteorological conditions and wind regime responsible for CDCL formation.

2. Background

2.1. Geographical conditions

The current study area lies in the northwestern Sichuan Basin and adjacent areas (Fig. 1). The Sichuan Basin (450–650 m asl–above sea level) is one of large basins in China, and is surrounded by the eastern Tibetan Plateau (2000–4500 m asl) to the west, the Yunnan–Guizhou Plateau (1400–1800 m asl) to the south, the Huaying Mountain (800–1000 m asl) to the east and the Qinling Mountains (2000–3000 m asl) to the north. Moreover, the Qinling Mountains, with east-to-west orientation, border the Chinese Loess Plateau to the north. The seismically active Longmen Mountains (Lungmenshan Mountains) thrust belt is located at the margin of the eastern Tibetan Plateau (Fig. 1C).

The Sichuan Basin consists of low hills and alluvial plains. Several major rivers, including the Minjiang River, Jialingjiang River, Tuojiang River and Fujiang River, flow into the northwestern part of the basin

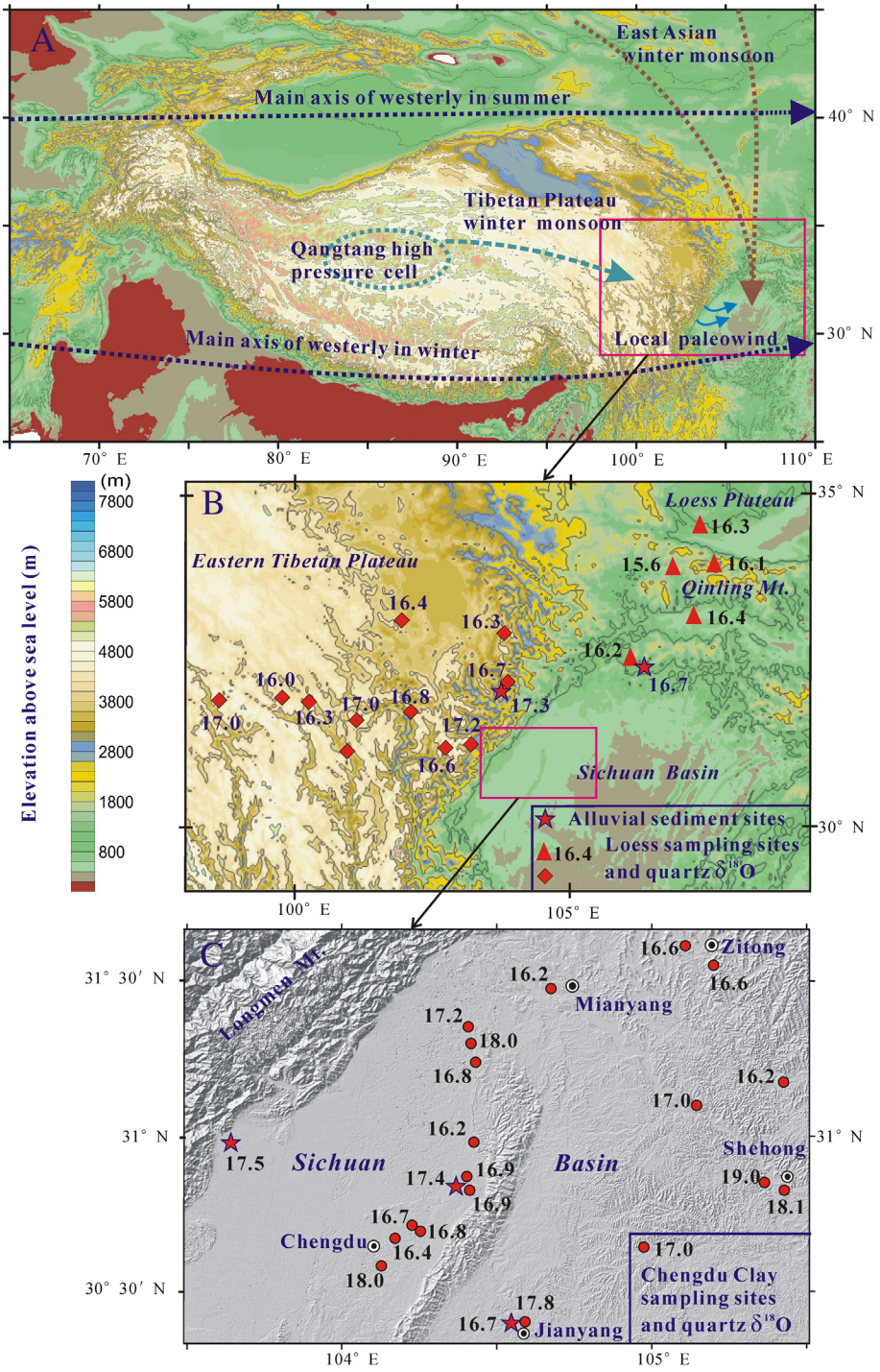

Fig. 1. A. Sketch map showing the topographic features and the potential atmospheric circulation for aeolian dust transport (main axes of the westerly jet are modified after Schiemann et al., 2009); B and C. sampling sites and the $\delta^{18}O$ values of quartz in the Chengdu Clay and adjacent loess.

and form various alluvial plains. The Sichuan Basin was cut by the Yangtze River near southern borders. All the above-mentioned rivers are tributaries of the Yangtze River.

The Sichuan Basin currently has a monsoon-influenced, humid, subtropical climate with four distinct seasons. The Qinling Mountains to the far north help shield the northwestern Sichuan Basin from the cold East Asian winter monsoon in the winter (Fig. 1B). The western Sichuan Basin has an annual average temperature of 16–17 °C. The average annual precipitation is 1000–1200 mm. Rainfall is greatest in July and August, and there is very little in the cooler months. Taking Chengdu city as a reference point, the dominant wind direction is static wind, with 43% annual frequency. NE and of NNE frequency throughout the year is 11%. The strong winds mainly occur during the summer. The average annual wind speed is about 1.1 m/s.

2.2. Geological setting

The developed Quaternary clayey strata in the northwestern Sichuan Basin can be divided into three units from top to bottom (Richardson, 1943; Shao et al., 1984; Zhang, 1988; Kong, 1994; Fig. 2A and B).

The upper horizon is CDCL (Fig. 2A). It forms a discontiguous blanket over the low hills and high river terraces in the western and northwestern Sichuan Basin (Thorp and Dye, 1936; Richardson, 1942, 1943; Liu, 1983). Fig. 1C shows the main distribution of the CDCL. The CDCL is brownish yellow in color (Munsell, 10YR 6/8) and is rich in calcareous concretions. The maximum thickness of the CDCL horizon is about 3 m. The underlying strata of the CDCL vary with various geophysical regions (Thorp and Dye, 1936; Richardson, 1942, 1943; Liu, 1983; Kong, 1994).

The middle horizon is brown clay with a dominant dark brown (7.5YR 5/6) or brownish yellow (10YR 6/8) color (Fig. 2A and B). Its thickness ranges from 1.5 to 6.0 m (Kong, 1994). Single pebbles occasionally occur in this horizon (Fig. 2C). It is rich in ferromanganese nodules. Calcareous concretions also occur within the top brown clay horizon. We observed that the ferromanganese nodules are often included within the calcareous concretions (Fig. 2D). The syntagmatic relationship of the ferromanganese nodules with the calcareous concretions indicates that part of the carbonate is leached and transported downward from the overlying CDCL and precipitates within the top brown clay horizon. Moreover, the CDCL unconformably overlies the brown clay (Fig. 2A).

The lower horizon consists of red clays with a dominant red color (2.5YR4/8). Its maximum thickness is about 6.0 m. The boundary between the red clay horizon and the overlying brown clay can be distinguished, even though recent weathering and reworking have blurred the boundary (Fig. 2B).

Throughout the profile, the CDCL and the underlying clay horizons exhibit a clayey texture, a massive and blocky structure and a lack of visible bedding features (Fig. 2A and B). A reticulately-mottled structure is developed within the brown clay (middle horizon) and red clay (lower horizon), filled with light gray clay (2.5Y 7/1; Fig. 2E).

At present, the term CDCL is given different stratigraphic meanings. Some scholars merge brown clay (middle horizon) and/or red clay (lower horizon) into the lithostratigraphic unit of the CDCL (Zhang, 1988; Kong, 1994; Qiao et al., 2007; Zhao et al., 2007; Han et al., 2010; Yang et al., 2010a, b). In the present paper, we follow the definition given primarily by Thorp and Dye (1936).

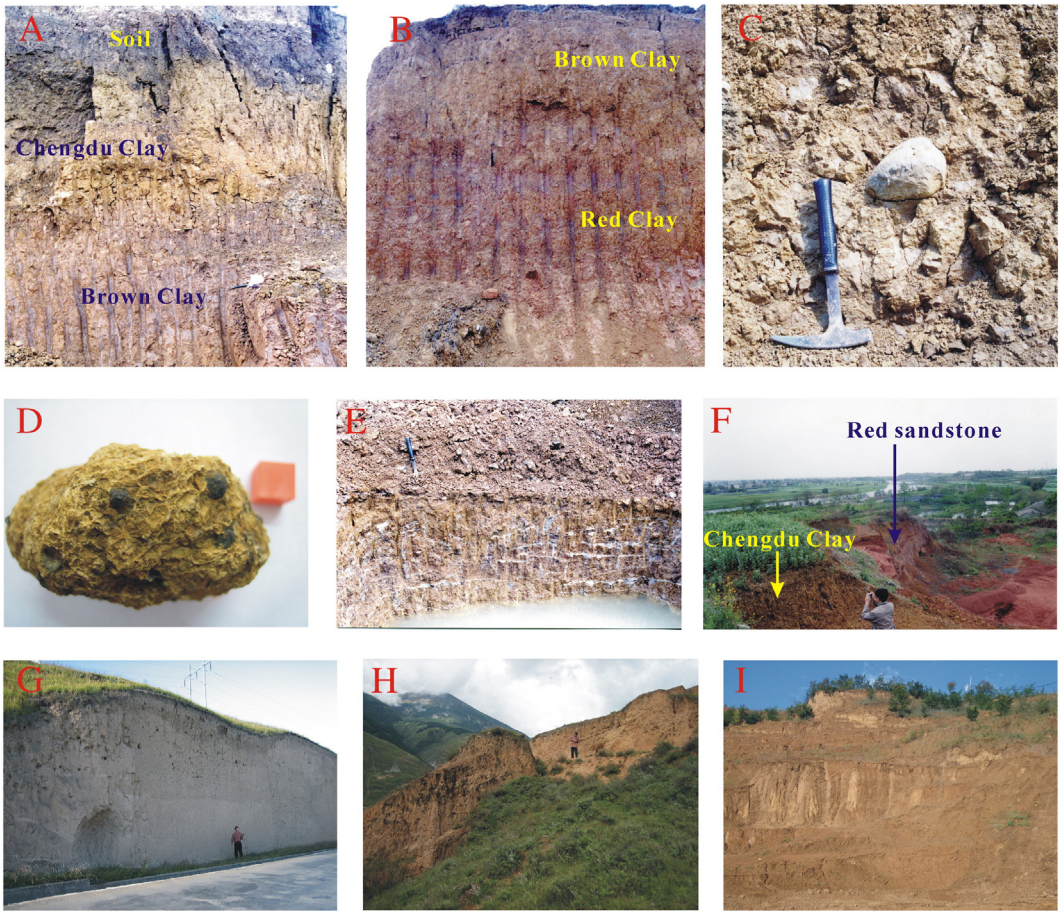

Fig. 2. Photographs of CDCL, ETPL and LPQL sections. A. CDCL covering the brown clay; B. the brown clay covering the red clay; C. pebble in the brown clay; D. a calcareous concretion occurring within the upper brown clay horizon (note the ferromanganese nodules being included in the calcareous concretion); E. the reticulately mottled structure of the lower red clay; F. CDCL covering Cretaceous red sandstone on a hill in the Sichuan Basin; G. Arba loess from the eastern Tibetan Plateau (3733 m asl). H. Daofu (Dawo) loess from the eastern Tibetan Plateau (3076 m asl); and I. Taibai loess from Qinling Mountains (1587 m asl).

Early investigators proposed that the CDCL formed within the Late Pleistocene based on stratigraphic correlation (Thorp and Dye, 1936; Richardson, 1942, 1943; Ma, 1944; Harland, 1945). More recently, the CDCL is identified as Late Pleistocene based on fossils and conventional ^{14}C dating (Liu, 1983; Chen and He, 1990) and lastly, based on optically stimulated luminescence (OSL) and ^{14}C dating methods, Yang et al. (2010a) and Han et al. (2010) proposed that the CDCL formed in the Late Pleistocene. Moreover, the red clay (lower horizon) began accumulating at about 825–1130 ka B.P. as shown by magnetostratigraphy (Zhao et al., 2007; Yang et al., 2010a).

2.3. Field sampling

Samples were collected from the CDCL and late Pleistocene ETPL and LPQL (Figs. 1 and 2). The samples were taken from 35 localities spanning 490 km in a south-north transect and 650 km in a west-east transect (Fig. 1). Additionally, the Minjiang River, Jialingjiang River, Tuojiang River and Bihe River form various fluvial plains in the western and northwestern part of the basin. Their fluvial sediments from floodplain and terrace were collected for comparison (Fig. 1). The Sichuan Basin is also known as the 'Red Basin' because of the Cretaceous red sandstone that is widely distributed (Fig. 2F). Thus, we collected one sample of weathered red sandstone for comparison. Detailed information about the sampling sites is listed in Appendix A.

3. Materials and methods

3.1. Quartz isolation

Quartz is the most common mineral in aeolian deposits. It weathers extremely slowly at the earth's surface (Götze and Zimmerle, 2000). Therefore, quartz grain size is used as a winter monsoon indicator (Xiao et al., 1995, 1997; Sun et al., 2006). The quartz oxygen isotopes (Hou et al., 2003; Feng et al., 2008), ESR (electron spin resonance) signal intensity and crystallinity of quartz (Sun et al., 2007b, 2008) are used as provenance tracers of Asian dust and Chinese loess.

Quartz was isolated from the aeolian, fluvial sediments and weathered red sandstone by sodium pyrosulfate ($Na_2S_2O_7$) fusion and a sequential treatment with solutions of 3 M HCl + 30% H_2SiF_6 + 0.1 M HF + saturated H_3BO_3 (Jackson et al., 1976).

3.2. Grain size measurement

The grain size distributions of bulk samples and the isolated quartz samples were examined by using a Malvern mastersizer-2000. Prior to measurement of the grain size distribution, the bulk samples were treated sequentially with 30% H_2O_2, 1.5 M HCl, addition of 10 ml 1% sodium hexametaphosphate ($(NaPO_3)_6$) dispersant and 90 s of ultrasonic dispersing. The quartz samples were measured after 30 s of ultrasonic dispersing. We calculated the mean quartz grain sizes, sorting, skewness and kurtosis parameters of all samples using the logarithmic method of moments (Blott and Pye, 2001).

3.3. Measurement of quartz oxygen isotope

The $\delta^{18}O$ of quartz depends on its formation temperature and the $\delta^{18}O$ of the source materials. Except through recrystallization, the $\delta^{18}O$ of quartz remains unchanged during surface processes, including diagenesis and alteration (Clayton et al., 1978). The $\delta^{18}O$ stability of quartz makes it a good source tracer (Feng et al., 2008).

To avoid grain-size effect on quartz oxygen isotope (Clayton et al., 1972; Gu et al., 1987; Hou et al., 2003; Feng et al., 2008), the same grain-size fractions (2–50 μm quartz grains) were isolated from typical samples for measurements of oxygen isotopes. The oxygen in the quartz was liberated by using the bromine pentafluoride (BrF_5) method (Clayton and Mayeda, 1963). Oxygen isotope ratios were determined by using a stable-isotope mass spectrometer (MAT-253 EM) installed at the Institute of Mineral Resources, Chinese Academy of Geological Sciences. The oxygen isotopic compositions are expressed as deviations relative to the Standard Mean Ocean Water (SMOW) reference ($\delta^{18}O = ([^{18}O/^{16}O]_{Sample}/[^{18}O/^{16}O]_{SMOW} - 1) \times 1000$). The analytical uncertainties are ±0.2‰.

3.4. Analysis of trace element concentrations

Trace elements are known to have different geochemical behaviors in mineral formation and in certain superficial processes. Ratios of elements with very different levels of incompatibility are especially useful in characterizing the composition and tracing the origin of aeolian dust (Taylor and McLennan, 1985; Cullers et al., 1988; Sun et al., 2007a; Muhs et al., 2008).

During dust transport and subsequent dust deposition, the dust grains undergo various degrees of dissolution and/or weathering. Unstable minerals (carbonate, halite, gypsum, etc.) decompose, and secondary Fe–Mn oxides and oxyhydroxides form, along with carbonate neoformation in the terrestrial dust deposits (e.g., loess and paleosols). Therefore, the stable silicate minerals provide more appropriate materials for tracing the dust provenance than bulk dust samples (Feng et al., 2009). To exclude the possible influence of such chemical alteration on trace elements, we removed the acid-soluble components by acid leaching.

Aeolian deposits and weathered red sandstone were treated with a 20% hydrochloric acid (HCl) solution at 97 °C in a Teflon vessel for 45 min (Yokoo et al., 2004). The silicate residues were washed four times with Milli-Q water. To avoid incorrect trace element determinations due to changing proportions of mineral interferences caused by grain size effects (Feng et al., 2011), grains partitioned from stable silicate minerals of the same size (2–50 μm) were isolated for typical samples based on Stokes' law (discarding the <2 μm fraction) and wet-sieving (discarding the >50 μm fraction).

The powder of the 2–50 μm fraction was dissolved by using the pressurized acid digestion method following the analytical procedures described by Qi et al. (2000). The concentrations of rare earth elements (REEs) and other trace elements in these samples were determined by using the inductively coupled plasma mass spectrometer (ICP-MS; X-7 series; Thermo Elemental) installed at the Institute of Tibetan Plateau Research, Chinese Academy of Sciences.

3.5. Analysis of $^{147}Sm/^{144}Nd$ ratio

Two representative samples subjected to the same pretreatment as the trace element samples, the Chengdu Clay (JTW1-3) and the Garze loess (GZ1-2) collected from the terrace of the Yalong River on the eastern Tibetan Plateau were further separated into seven gain size fractions (<2 μm, 2–5 μm, 5–10 μm, 10–20 μm, 20–32 μm, 32–50 μm and >50 μm fractions) based on Stokes' Law with sequential extraction. The Sm and Nd concentrations and $^{147}Sm/^{144}Nd$ ratios of the whole silicate minerals (WS) and the seven grain size fractions were determined by using isotope dilution analysis (Feng et al., 2010).

4. Results

4.1. Grain size composition of the bulk Chengdu Clay

Fig. 3 illustrates the grain size distributions of the bulk Chengdu Clay samples. These results indicate that the bulk Chengdu Clay is composed mainly of silt and fine-sand grains (about 2–100 μm). The component of silt (2–50 μm) sized grains accounts for 64 to 96% of the total. The component of clayey grains (<2 μm) varies from 0.3 to 28.5%. In addition, most samples of bulk CDCL contain small components with a modal size of 150–200 μm. The grain size distribution shows unimodal or bimodal patterns.

4.2. Quartz contents and quartz grain size distribution

The results of quartz grain size distributions and quartz contents are shown in Figs. 4 and 5 and Appendix A; while spatial variations of the quartz granulometric composition and the quartz content are illustrated in Figs. 6 and 7.

The data illustrated in Fig. 4 indicate that all aeolian samples are mainly composed of silt-sized (2–50 μm) quartz grains. This similarity between the CDCL and typical aeolian loess provides new evidence for an aeolian origin of the CDCL. However, there are two significant differences: (1) CDCL is finer in the modal size than ETPL and LPQL (Figs. 4, 6C and 7B); and (2) many samples of CDCL contain a component with a modal size of 200–300 μm, which is lacking in ETPL and LPQL (Fig. 4). There are no significant differences in quartz contents of aeolian samples among the three regions (Figs. 5, 6A and 7D). The weathered red sandstone is characterized by high quartz content (63.2%; Fig. 5; Appendix A). The grain size distribution of quartz in the weathered red sandstone presents a wide range of 1–800 μm, but it is mainly composed of sand-sized (100–800 μm) quartz grains (Fig. 4C; Appendix A).

4.3. Quartz oxygen isotopes

Figs. 1 and 5 and Appendix A present the $\delta^{18}O$ of 2–50 μm quartz fractions for CDCL, ETPL, LPQL, alluvial sediments and the weathered red sandstone. For ETPL, the $\delta^{18}O$ values vary from 16.0‰ to 17.2‰ with a mean value of 16.6‰ ($n = 11$). The $\delta^{18}O$ values of LPQL vary from 15.6‰ to 16.4‰ with a mean value of 16.1‰ ($n = 5$). Correspondingly, the $\delta^{18}O$ values of CDCL range from 16.2‰ to 19.0‰ with a mean value of 17.1‰ ($n = 18$). The results show that the $\delta^{18}O$ values of quartz of CDCL are higher than those of ETPL and LPQL (Figs. 1 and 5). The samples of CDCL also show a large degree of spatial variation in the quartz $\delta^{18}O$ values (Fig. 5).

In the five alluvial sediments, the $\delta^{18}O$ values of quartz vary from 16.7‰ to 17.5‰ with a mean value of 17.1‰ ($n = 5$), which is similar to the mean value of CDCL (see Appendix A and Fig. 1). The $\delta^{18}O$ value of quartz from the weathered red sandstone is 17.6% (Fig. 5; Appendix A). This value is higher than those of most of aeolian deposits (Fig. 5).

4.4. REEs and other trace elements

The analytical results of trace element concentrations for the 2–50 μm fractions are listed in Appendix B. The results show that all CDCL samples have total REE concentrations (ΣREE) in the range of 118–144 μg/g, which is significantly lower than the values of 146–217 μg/g for ETPL. Moreover, the concentration of each REE and Y in CDCL is systematically lower than that in ETPL. By contrast, there is no great distinction between CDCL and LPQL for the total REE, individual REE or Y concentrations (Appendix B).

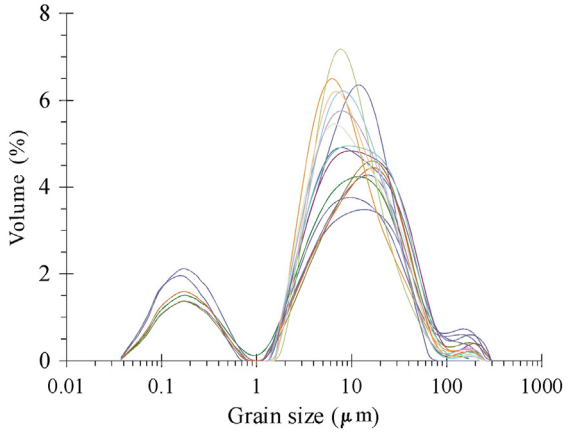

Fig. 3. Grain size distribution of the bulk Chengdu Clay.

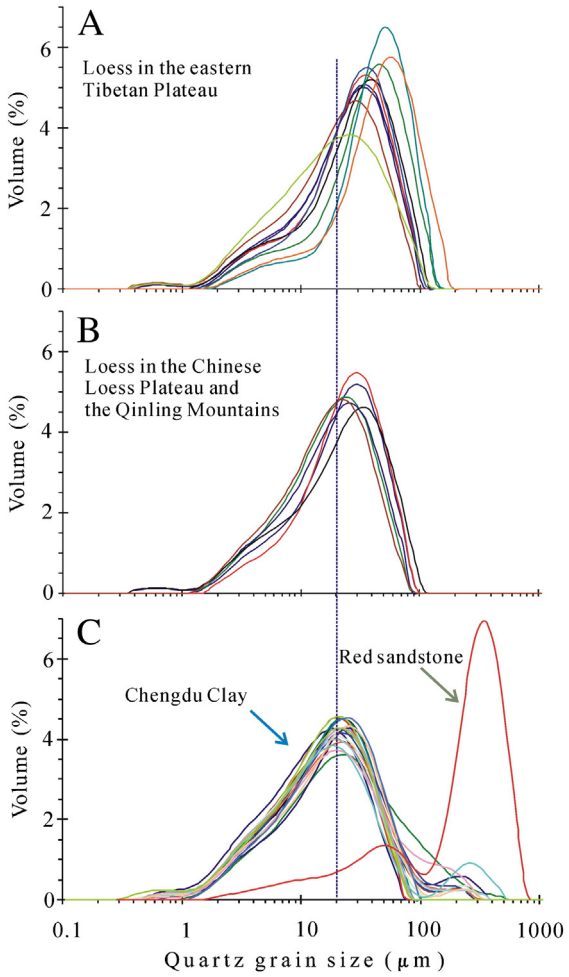

Fig. 4. Quartz grain size distribution of (A) ETPL; (B) LPQL; (C) CDCL and weathered red sandstone.

Chondrite-normalized REE patterns for CDCL, ETPL and LPQL are shown in Fig. 8. All REE patterns are remarkably similar in shape, with light REE enrichments, relatively flat heavy REE profiles and consistent negative Eu anomalies. This is further evidence that CDCL is derived from aeolian deposits. In addition, the features of REE fractionation for CDCL, ETPL and LPQL differ from each other. In diagrams of ΣREE vs. $(Ga/Yb)_N$ and $(La/Sm)_N$ vs. $(Ga/Yb)_N$, the data fall into three fields (Fig. 9).

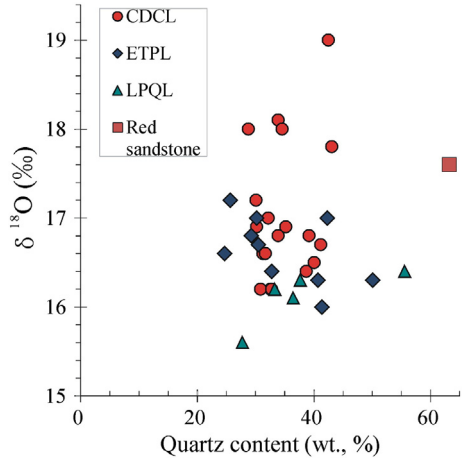

Fig. 5. Variations of the quartz contents and quartz $\delta^{18}O$ values in CDCL, ETPL, LPQL and weathered red sandstone.

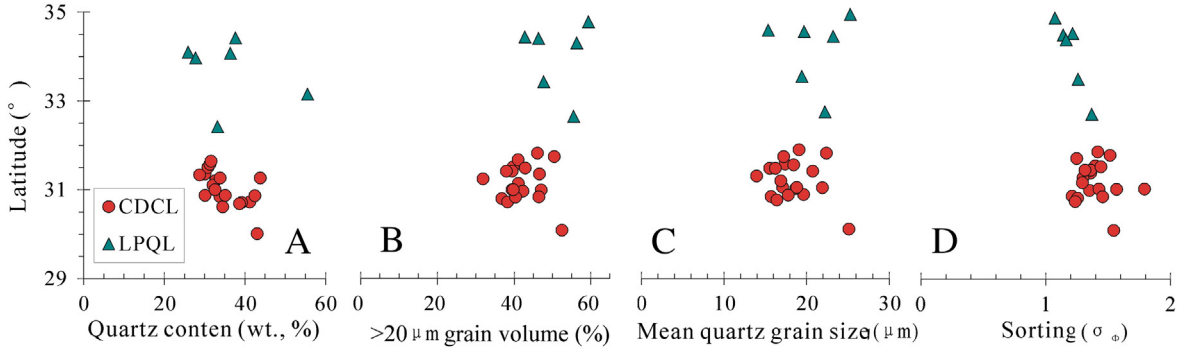

Fig. 6. Spatial variations of quartz content and quartz granulometric composition along with latitude for CDCL and LPQL.

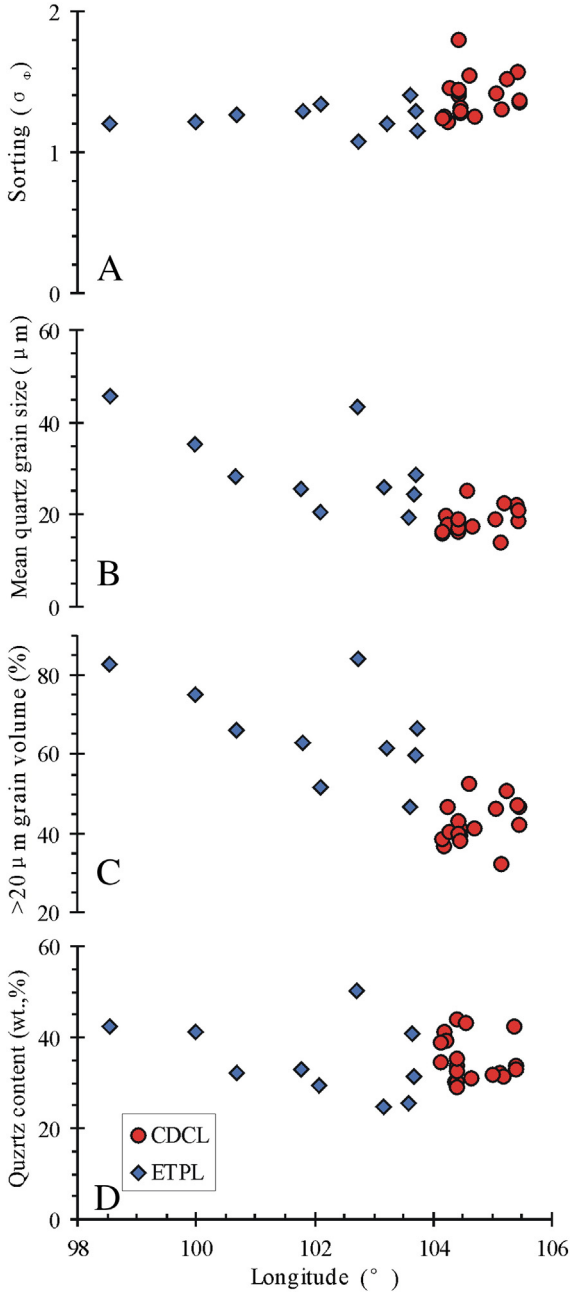

Fig. 7. Spatial variations of quartz content and quartz granulometric composition along with longitude for CDCL and ETPL.

Compared with ETPL, the CDCL have higher concentrations of Li, Ti, Co, Ni, Cu, Zn, As and Cs, lower concentrations of Be, B, Sc, V, Rb, Sr, Zr, Ba, Hf, Pb, Th and U and similar concentrations of Cr, Ga, Nb, Sn, Ta and Tl (Appendix B). By contrast, the CDCL have higher concentrations of Li, B, Ti, Co, Ni, Cu, Zn, Zr, Cs and Hf, lower concentrations of Be, Sc, V, Rb, Sr and Ba and similar concentrations of Cr, Ga, As, Nb, Sn, Ta, Tl, Th and U, compared with LPQL. Generally, most of the trace elements show distinct compositional fields for CDCL, ETPL and LPQL (Appendix B).

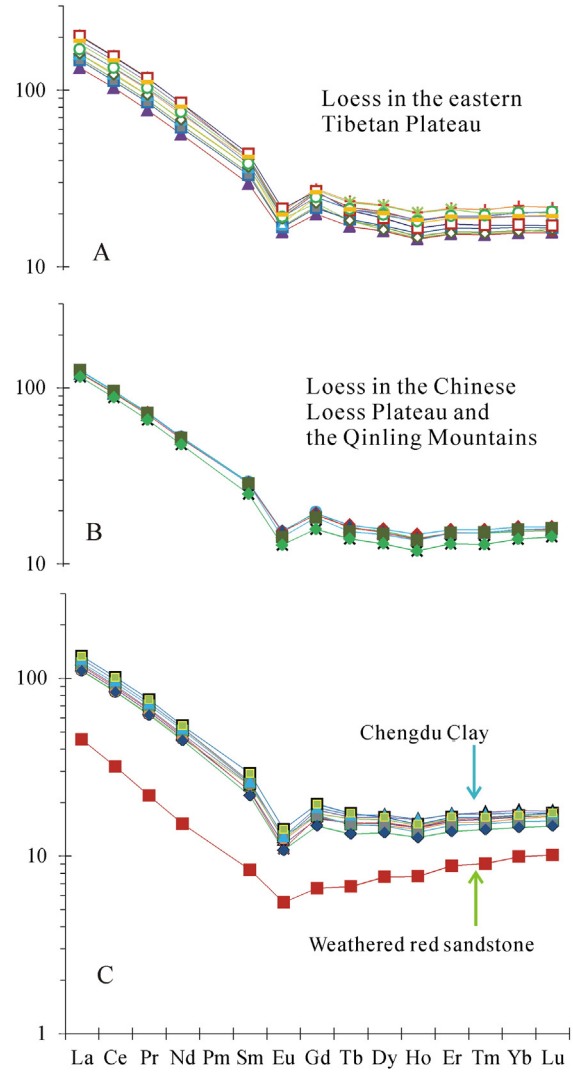

Fig. 8. Chondrite-normalized REE distribution patterns of (A) ETPL; (B) LPQL; and (C) CDCL and weathered red sandstone (C1 chondrite data after Anders and Grevesse, 1989).

Fig. 10 presents the trace element geochemistry of CDCL, ETPL and LPQL as bivariate plots of Th/Sc vs. Sm/La, Rb/Sr vs. Ba/Sr and U/Pb vs. Th/U. The data are somewhat scattered, but it is clear that they show systematic trends. In the three diagrams, CDCL plots mostly outside the fields of ETPL and LPQL (Fig. 10).

The concentrations of each REE (especially light REE) and Y in the weathered red sandstone are significantly lower than those in CDCL (Appendix B; Fig. 8). Moreover, the weathered red sandstone has significantly lower concentrations of Li, B, Ti, Cr, Rb, Sr, Zr, Ba, Th and U, and higher concentrations of V, Cu, Zn, Ga and Pb, compared with CDCL (Appendix B).

4.5. Sm–Nd isotopic system in various grain size fractions

The $^{147}Sm/^{144}Nd$ ratios of various grain size fractions in CDCL (JTW1-3) and ETPL (GZ1-2) are presented in Appendix C. The $^{143}Nd/^{144}Nd$ data for the same grain size fractions from CDCL (JTW1-3), ETPL (GZ1-2) and LPQL (LT-25) after Feng et al. (2009, 2010) are also presented here for comparison (Appendix C). The plot of the $f^{Sm/Nd}$ (deviation of $^{147}Sm/^{144}Nd$ from a chondritic uniform reservoir) values vs. the T_{Nd} (Nd model ages) values indicates that the variations of CDCL (JTW1-3) and ETPL (GZ1-2) with grain size differ systematically from that of LPQL (LT-25; Fig. 11 and Appendix C). The Nd model ages (T_{Nd}) associated with various grain sizes indicate that the CDCL (JTW1-3) and ETPL (GZ1-2) reported here have more juvenile components than those of LPQL (LT-25) (Fig. 11; Appendix C). Correspondingly, some fractions of the CDCL (JTW1-3) and ETPL (GZ1-2) display similar $f^{Sm/Nd}$ values and Nd model ages.

5. Discussion

5.1. Aeolian dust transport mechanisms

Three possible mechanisms for dust transport to the Sichuan Basin have been proposed (Fig. 1A). One is through surface winds of the East Asian winter monsoon (Ma, 1944; Lu et al., 1976; Wang, 1998). Another is through the westerly jet and/or Tibetan Plateau winter monsoon winds (Fang, 1995; Yang et al., 2010a,b). The last is local, small-scale and near-surface wind (Feng et al., 2010, 2011; Hu et al., 2010). Accordingly, the potential source areas for CDCL include the arid area in northwestern China and/or Inner Mongolia, the west and central Tibetan Plateau and the northwestern Sichuan Basin.

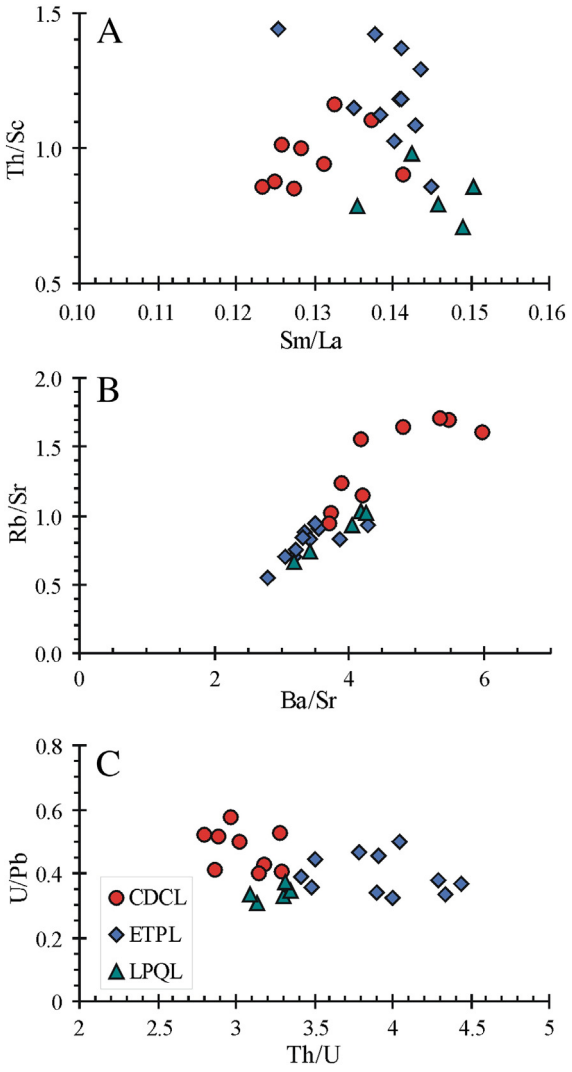

Fig. 10. (A) Th/Sc vs. Sm/La, (B) Rb/Sr vs. Ba/Sr, and (C) U/Pb vs. Th/U diagrams comparing CDCL, ETPL, and LPQL.

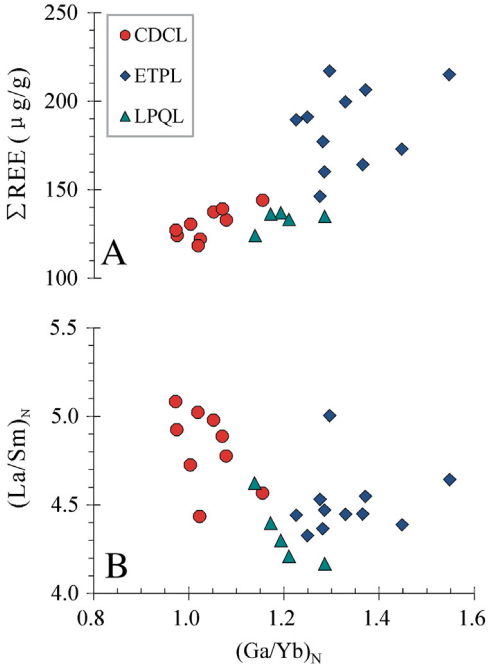

Fig. 9. $(Ga/Yb)_N$ vs. $(La/Sm)_N$ and total REE concentration (ΣREE) for CDCL, LPQL, and ETPL. *N* inferred C1 chondrite-normalized (chondrite data after Anders and Grevesse, 1989).

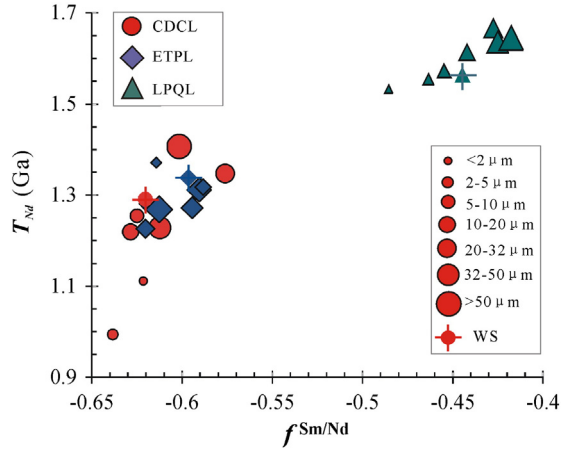

Fig. 11. Plot of $f^{Sm/Nd}$ vs. T_{Nd} for CDCL (JTW1-3), ETPL (GZ1-2) and LPQL (LT-25; after Feng et al., 2009) with the whole silicate minerals (WS) and the various grain size fractions.

5.1.1. East Asian winter monsoon

The East Asian winter monsoon is derived from thermal differences between the land and the sea. For understanding the transport mechanisms of loess on the Chinese Loess Plateau, a basic consensus has been achieved, i.e. loess on the Chinese Loess Plateau is mainly transported by low-level circulation of the East Asian winter monsoon. The Qinling Mountains are located between the Chinese Loess Plateau and the Sichuan Basin (Fig. 1). Their altitudes range from 2000 to 3000 m asl. The highest peak in the range is Mount Taibai at 3767 m asl. The Qinling Mountains as a topographic obstacle to the East Asian winter monsoon, prevent effectively much of the aeolian dust from reaching the Sichuan Basin. However, part of dust can still be transported over the Qinling Mountains and be deposited in the basin.

5.1.2. Tibetan Plateau winter monsoon

Arid and semi-arid zones of the central and western Tibetan Plateau are potential source areas of the aeolian dust. The aeolian dust transported by the Tibetan Plateau Monsoon is mentioned by many researchers (Fang, 1995; Lu et al., 2004; Lü et al., 2004; Yang et al., 2010a,b). However, the surface deflation, dust storm formation and especially aeolian dust transport need favorable meteorological conditions.

Some scholars have proposed that a separate, relatively shallow, monsoon exists on the Tibetan Plateau (Xu and Gao, 1962; Tang and Reiter, 1984; Tang, 1998). However, the meteorological characteristics of the Tibetan Plateau Monsoon are not fully clear.

It is suggested that the Tibetan Plateau Monsoon is generated from a cold high pressure center and a warm low pressure center on the Qangtang Plateau during winter and summer, respectively (Fig. 1A). Above the near-surface wind system, a seasonally reversing wind occurs as the Tibetan Plateau Monsoon system (Tang, 1998). Tang (1998) proposed that the wind system on the Tibetan Plateau includes three layers. The lowest level is a near-surface wind system with thickness less than 1000 m. The intermediate level is the Tibetan Plateau Monsoon system with thickness less than 3000 m, while the upper layer is the planetary wind system. Thus, the Tibetan Plateau Monsoon is not a near-surface wind system. In addition, the Tibetan Plateau Monsoon does not result from a land-sea thermal difference. To summarize the above discussion, a suggestion can be made that the eastward Tibetan Plateau winter monsoon cannot transport aeolian dust of >20 μm in diameter over long distances, even if it exists. Correspondingly, the CDCL samples contain a large number of >20 μm grains (Figs. 3 and 4).

5.1.3. Westerly jet

Schiemann et al. (2009) demonstrated that during winter and summer the westerly jet is located, respectively, to the south and north of the Tibetan Plateau (Fig. 1A). During the spring and autumn seasons the jet shifts from south to north and vice versa. The spring shift is associated with large interannual variations. During northward migration in April/May, the jet intensity weakens and its latitudinal position varies considerably. In some springs, there are several shifts and split configurations that occur before the jet settles in its northern summer position (Schiemann et al., 2009).

It is suggested that the cold climate had stronger winds, which may have caused greater entrainment and more efficient transport of dust (Hesse and McTainsh, 1999; Moreno et al., 2002). During glacial and stadial periods, however, there is evidence of changes in vegetation (Moreno and León, 2003; Ono and Irino, 2004) and provenance of aeolian dust (Nagashima et al., 2007, 2011), and global climate models (Yin, 2005; Williams and Bryan, 2006; Toggweiler and Russell, 2008) demonstrate that the main axes of the westerly jet in both the northern and southern hemispheres shift in latitude toward the equator. Nagashima et al. (2011) further suggested that a westerly jet axis should locate to the south of the Tibetan Plateau throughout most of the year during glacial and stadial periods. This idea appears to be supported by dust flux records in the northwestern Pacific. Rea and Leinen (1988) found that the maximum in dust flux occurred 6000 yr B.P. at the Holocene climatic optimum, whereas dust inputs at present and at 18,000 yr B.P., the time of the last glacial maximum, are moderately low in the pelagic deposits. Thus, rates of dust deposition in the northwestern Pacific and the Chinese Loess Plateau show a poor correlation during the last 30,000 yr B.P. (Pye and Zhou, 1989). Many reasons, such as a dry mid-Holocene (Rea and Leinen, 1988; Chen et al., 2003) and different patterns of atmospheric circulation (Pye and Zhou, 1989), have been given to explain the differences in the timing of the dust flux maximum between the continent and the northwestern Pacific, where dust originates mainly from Inner Asia. We suggest that the westerly jet axis shifting to the south of the Tibetan Plateau throughout most of the year during glacial periods, and then being far away from the dust source area in northwestern China and/or Inner Mongolia, can explain the observations.

The position of the westerly jet axis in relation to the dust source area on the Tibetan Plateau is also a critical factor. When the westerly jet axis is aligned with the dust source area, it gives rise to more dust transport from the interior of the Tibetan Plateau. If it is far away from the interior of the Tibetan Plateau and is poorly aligned with the dust source area, it would bring less dust downwind. Because the main axis of the westerly jet is not directly over the interior of the Tibetan Plateau during glacial and stadial periods, we propose that dust transport by the westerly jet is not important, especially for the formation of the CDCL.

5.1.4. A katabatic wind

The Sichuan Basin to the west is adjacent to the eastern margin of the Tibetan Plateau (2000–4500 m asl). The highest peak in this range is the Minya Konka at 7556 m asl. The topographic margin of the Tibetan Plateau is one of the world's most remarkable continental escarpments (Kirby et al., 2002). The steep topographic escarpment adjacent to the Sichuan Basin has been deeply dissected by the Minjiang River and other rivers, which have produced high-relief, narrow river gorges and threshold hillslopes (Kirby et al., 2002; Ouimet et al., 2007). During glacial and stadial periods, an ancient katabatic wind that originated from the eastern margin of the Tibetan Plateau probably occurred.

Aeolian deflation by katabatic winds is also a significant transport mechanism for loess in cold areas (Thorson and Bender, 1985; Muhs and Budahn, 2006; Schaetzl and Attig, 2013). The katabatic wind possibly rushed at high speeds down the steep topographic escarpment on the eastern margin of the Tibetan Plateau. Thus, the entire near-surface wind field over the northwestern Sichuan Basin was largely determined by the westerly katabatic wind during glacial and stadial periods.

If this model is valid, it suggests that a predominant westerly katabatic wind becomes strong enough to effectively remove dust from the surface and re-accumulate the eroded dust mass within the surrounding eastern areas. The alluvial plain and alluvial–proluvial fan in the northwestern Sichuan Basin regions may be significant dust sources for the CDCL.

Based on the points discussed above, it is suggested that the East Asian winter monsoon and an ancient katabatic wind are potentially significant transport mechanisms for the dust deposition in the western Sichuan Basin. As to which one is more important is discussed below.

5.2. Spatial variation and dust transport path

During aeolian dust transport, sorting by winds leads to spatial variations in the grain size of aeolian deposits (Pye, 1987; Tsoar and Pye, 1987). This, in turn, leads to grain-size-dependent changes in mineral assemblages and geochemical components (Rex et al., 1969; Clayton et al., 1972; Miao et al., 2004; Hao et al., 2010; Feng et al., 2011). In contrast, $^{143}Nd/^{144}Nd$ isotope ratios do not depend on grain size for homogeneous loess, while $^{147}Sm/^{144}Nd$ ratios and the $f^{Sm/Nd}$ values tend to increase with increasing grain size (Feng et al., 2009). The T_{Nd} values of aeolian deposits generally reflect the average crustal residence ages of the rocks in the source terrain (Taylor et al., 1983; Goldstein, 1988).

Accordingly, the Nd model ages have been used to trace the provenance of aeolian deposits (Feng et al., 2009 and references therein).

If there are original relationships among CDCL, ETPL and LPQL, the spatial variations or spatial consistency for different fingerprints should be identified, and the above inference should be supported by the following evidence: (1) a progressive decrease in the mean quartz grain size of aeolian deposits with distance from the source should occur; (2) the distribution of grain size of aeolian deposits should show evidence of significant sorting during transport; (3) the content of >20 μm sized quartz grains should decrease toward the Sichuan Basin; (4) CDCL should be composed mainly of fine silt and clayey grains (<20 μm), which are transported in long-term suspension; (5) the quartz content should tend to decrease downwind due to enhanced clay content in the fine component; (6) the quartz $\delta^{18}O$ and other geochemical indices within the same size fractions should have little spatial variation; and (7) the $^{143}Nd/^{144}Nd$ isotopic ratios should exhibit little variation with grain size, whereas $^{147}Sm/^{144}Nd$ ratios, $f^{Sm/Nd}$ and T_{Nd} values should have little variation with the same size fractions.

In fact, most of our results do not follow the above rules (Figs. 3–11). These significant differences indicate that the potential sources for CDCL, ETPL and LPQL probably differ from one another. In addition, the assumption of CDCL transport by the Tibetan Plateau Monsoon and/or westerly jet and the East Asian winter monsoon is not supported by most of the evidence. Many samples of CDCL indeed contain more components of clayey grains (<2 μm) than ETPL and LPQL. However, clayey grains vary under weathering processes. The clayey grains in CDCL may be mainly derived from the pedogenesis processes, which are favored by the sub-tropical climate in the Sichuan Basin. These processes would have caused the formation of secondary clay minerals after aeolian deposition. Therefore, the enrichment of clayey grains in CDCL cannot be used as evidence of long distance transport.

Correspondingly, the CDCL is probably derived from a local source (Richardson, 1942; Feng et al., 2010, 2011; Hu et al., 2010). An ancient katabatic wind during glacial and stadial periods possibly played an important role in the dust transport. This inference is supported by the following evidence. (1) The bulk and quartz samples of CDCL often contain 150–300 μm components (Figs. 3 and 4). In general, grains of this size are transported by wind only by saltation and cannot be blown long distances (Pye, 1987). We infer that parts of the coarse-grained components in some CDCL may be derived from the weathered red sandstone, which is widely distributed in the Sichuan Basin (Figs. 4C and 5). (2) The $\delta^{18}O$ values of quartz in the CDCL range from 16.2‰ to 19.0‰, and vary significantly with geographical location. This variation indicates that dust sources for CDCL were not very well mixed, and were not very homogeneous in composition (Figs. 1 and 5).

6. Conclusions

Given the above observations, we suggest that the CDCL in the northwestern Sichuan Basin examined in this work is of aeolian origin with weathering reworking. The dust sources of CDCL differ from those of ETPL and LPQL. Most lines of evidence indicate that an ancient katabatic wind during glacial and stadial periods, possibly is a significant transport mechanism for the dust deposition in the western Sichuan Basin. There is little possibility of an effective aeolian transport system bringing dust from the Tibetan Plateau, the arid area in northwestern China and/or Inner Mongolia into the Sichuan Basin, where it may be deposited and accumulated as CDCL. Thus, long-range-transported dust possibly plays a minor role in controlling the magnitude of the dust flux to the CDCL in the Sichuan Basin. Correspondingly, CDCL is possibly transported by an ancient katabatic wind over a short distance. The alluvial plain and alluvial–proluvial fan in the northwestern Sichuan Basin regions may be a significant dust source for the CDCL. The existence of an aeolian origin of CDCL is evidence for wind erosion and suggests that the surface in the northwestern Sichuan Basin was a windier environment in the past than at present.

Acknowledgments

We thank the anonymous reviewers for their critical comments. This work was supported by the National Natural Science Foundation of China (NSFC; grant no. 41171008, 40771028).

Appendix A

Sampling location, quartz content, quartz oxygen isotope, and quartz granulometric composition for the Chengdu Clay, the loess from the eastern Tibetan Plateau, the loess from the Chinese Loess Plateau and the Qinling Mountains, alluvial sediments and weathered red sandstone.

Sample no.	Sampling depth (m)	Location		Altitude (m a.s.l.)	Quartz content (wt.%)	$\delta^{18}O$ of 2–50 μm quartz fractions (‰)	Quartz grain size distribution (volume, %)								Mean quartz grain size (μm)	Sorting (σ_Φ)
		Latitude	Longitude				<2 (μm)	2–10 (μm)	10–20 (μm)	20–32 (μm)	32–50 (μm)	50–63 (μm)	63–100 (μm)	>100 (μm)		
Chengdu Clay																
DT1-2	0.43	31°6.337′	105°6.708′	496	32.2	17.0	4.7	35.2	28.1	18.3	10.7	2.5	0.5	0.0	14.0	1.30
JY1-1	0.70	30°23.050′	104°33.845′	411	43.1	17.8	1.3	23.8	22.4	16.9	13.4	5.5	8.1	8.6	25.1	1.55
CDST-2	0.90	30°40.682′	104°8.545′	545	38.7	16.4	3.4	31.2	28.6	20.3	12.7	3.1	0.7	0.0	15.7	1.26
HY1-1	0.30	31°34.125′	105°10.480′	458	31.3	16.6	2.4	23.6	23.5	20.0	15.4	5.0	4.4	5.8	22.4	1.52
LS1-1	1.00	30°59.96′	104°23.931′	478	32.6	16.2	3.3	28.8	26.7	20.8	14.4	4.0	2.0	0.0	16.9	1.30
CYC1-1	0.60	31°21.090′	104°23.257′	554	30.1	17.2	2.7	31.5	26.0	18.0	12.3	3.8	3.4	2.3	17.4	1.40
PM1-1	0.30	31°29.403′	104°38.807′	544	30.9	16.2	2.4	29.3	27.2	20.8	14.3	4.0	2.0	0.0	17.2	1.25
BSC1-1	0.70	30°50.532′	105°24.695′	358	33.9	18.1	2.0	28.8	26.8	19.3	13.1	4.0	3.5	2.5	18.7	1.35
SZS1-3	1.00	30°36.404′	104°7.198′	505	34.6	18.0	2.9	30.2	28.6	20.6	13.2	3.3	1.2	0.0	16.4	1.24
LP2-3	0.35	31°19.832′	104°23.555′	551	28.8	18.0	2.9	29.6	24.6	18.2	13.4	4.4	4.2	2.9	22.4	1.45
JT3-1	0.60	30°51.904′	104°23.142′	454	30.2	16.9	3.2	31.3	25.9	18.5	12.6	3.6	2.5	2.3	17.1	1.43
YT1-1	0.40	31°12.274′	105°24.353′	383	32.8	16.2	1.3	26.6	25.4	19.3	14.3	4.8	4.9	3.4	20.8	1.36
TSH1-1	0.65	30°42.509′	104°13.706′	487	39.2	16.8	3.2	30.4	25.9	17.9	12.0	3.8	3.7	3.1	17.8	1.46
SSH1-1	0.35	30°51.802′	105°22.202′	344	42.5	19.0	2.1	26.9	23.8	16.9	12.1	4.3	5.9	7.9	21.9	1.57
HXXH-7	2.10	31°14.695′	104°24.865′	516	33.9	16.8	3.6	30.8	26.1	19.8	13.9	4.0	1.8	0.0	16.2	1.32
SH1-6	0.55	31°38.513′	105°5.295′	502	31.7	16.6	3.1	26.5	24.3	20.3	15.4	4.8	3.6	2.0	19.1	1.42
SLC1-3	1.70	30°42.919′	104°11.545′	524	41.2	16.7	1.2	26.1	26.2	21.2	16.1	5.2	4.0	0.0	19.7	1.21
JTW1-3	0.70	30°51.9863′	104°23.5923′	451	35.2	16.9	4.5	30.4	25.2	16.7	10.4	2.8	1.7	8.3	18.8	1.80
HX1-50	0.80	31°15.433′	104°24.596′	524	40.1	16.5	4.7	30.4	26.8	19.6	13.3	3.7	1.4	0.0	15.6	1.28

Appendix A (*continued*)

Sample no.	Sampling depth (m)	Location		Altitude (m a.s.l.)	Quartz content (wt.%)	$\delta^{18}O$ of 2–50 μm quartz fractions (‰)	Quartz grain size distribution (volume, %)								Mean quartz grain size (μm)	Sorting (σ_ϕ)
		Latitude	Longitude				<2 (μm)	2–10 (μm)	10–20 (μm)	20–32 (μm)	32–50 (μm)	50–63 (μm)	63–100 (μm)	>100 (μm)		
Loess from the eastern Tibetan Plateau																
LX1-3	1.10	31°27.165′	103°9.989′	2055	24.7	16.6	0.5	17.7	20.0	21.8	21.9	8.8	8.9	0.4	26.1	1.20
GZ1-2	2.50	31°37.151′	99°58.643′	3431	41.4	16.0	0.3	12.3	12.3	17.9	24.2	12.3	16.9	3.8	35.2	1.22
AB1-1	0.60	32°54.405′	101°46.344′	3373	32.8	16.4	1.9	16.6	18.5	22.2	23.0	9.2	8.6	0.1	25.5	1.29
SP1-2	0.45	32°47.469′	103°39.219′	3197	40.7	16.3	1.7	18.8	20.0	21.6	21.5	8.4	7.9	0.1	24.3	1.29
SLH1-1	0.60	31°24.392′	100°40718′	3259	30.2	17.0	0.8	16.7	16.4	20.3	23.0	10.1	11.7	1.0	28.1	1.27
JC1-1	0.80	31°29.771′	102°4.891′	2484	29.3	16.8	2.7	22.7	22.7	21.5	18.6	6.6	5.1	0.0	20.6	1.34
WQ1-2	0.75	33°6.337′	102°42.575′	3478	50.1	16.3	0.0	7.7	8.3	15.7	26.1	14.9	22.0	5.2	43.3	1.07
MX2-4	1.56	32°0.296′	103°41.014′	2380	30.5	16.7	0.4	14.4	18.6	22.7	24.0	9.8	9.9	0.4	28.6	1.15
WC1-2	1.20	31°27.745′	103°34.913′	1882	25.7	17.2	2.7	27.5	23.2	18.0	15.2	5.9	6.8	0.7	19.4	1.40
GT1-5	1.90	31°42.418′	98°32.895′	3110	42.3	17.0	0.1	8.9	8.4	13.2	21.9	13.4	22.8	11.4	45.8	1.21
DF1-1	0.50	31°0.009′	101°5.987′	3076												
Loess from the Chinese Loess Plateau and the Qinling Mountains																
FZ1-1	0.50	33°58.325′	106°38.479′	1053	27.8	15.6	0.8	19.7	23.2	23.6	20.8	7.1	4.9	0.0	23.2	1.17
LJG1-2	1.00	34°4.326′	107°18.677′	1587	36.5	16.1	0.9	25.0	27.7	22.7	16.7	4.9	2.2	0.0	19.7	1.14
WJP1-1	0.70	33°5.222′	106°56.771′	534	55.6	16.4	2.3	24.3	25.6	22.1	17.3	5.5	3.0	0.0	19.5	1.26
GJH1-3	1.20	32°25.348′	105°46.079′	480	33.3	16.2	2.5	21.7	20.2	20.3	19.8	7.8	7.5	0.2	22.2	1.37
LH1-3	5.75	34°25.394′	107°7.549′	908	37.7	16.3	0.3	16.4	23.9	24.9	21.8	7.5	5.2	0.0	25.3	1.08
LT-25*		34°6′	109°19′		26.0		1.1	27.5	28.5	22.2	15.0	3.9	1.8	0.0	15.4	1.22
Alluvial sediments from Jialingjiang River																
GJH1-13		32°25.348′	105°46.079′	480		16.7										
Alluvial sediments from Bihe River																
JT4-1		30°51.904′	104°23.142′	454		17.4										
Alluvial sediments from Tuojiang River																
JYTJ-1		30°23.782′	104°33.284′	380		16.7										
Alluvial sediments from Minjiang River																
MJ-1		30°58.933′	103°36.563′	717		17.5										
Alluvial sediments from terrace of Minjiang River																
MX1-1		32°4.641′	103°42.913′	3070		17.3										
Weathered red sandstone																
JTW1-8	2.65	30°51.9863′	104°23.5923′	451	63.2	17.6	0.1	4.7	4.0	4.0	5.6	3.1	4.3	74.2	199	1.83

* Data after Feng et al., 2008.

Appendix B

Mean concentrations (μg/g) of rare earth elements and other trace elements in the 2–50 μm fractions from CDCL, ETPL, LPQL and the weathered red sandstone.

Elements	CDCL ($n = 9; \pm\sigma$)	ETPL ($n = 11; \pm\sigma$)	LPQL ($n = 5; \pm\sigma$)	Weathered red sandstone
Li	42.6 ± 5.5	24.6 ± 4.9	26.2 ± 5.4	24.9
Be	1.18 ± 0.08	1.89 ± 0.24	1.54 ± 0.24	1.35
B	81.6 ± 5.4	85.3 ± 13.6	67.4 ± 8.9	41.6
Sc	8.97 ± 0.85	10.5 ± 1.2	10.3 ± 0.8	8.71
Ti	5795 ± 203	5340 ± 245	5386 ± 213	3627
V	62.7 ± 5.6	72.6 ± 9.7	69.4 ± 6.1	79.9
Cr	59.6 ± 5.9	60.5 ± 5.5	57.3 ± 3.6	48.9
Co	2.30 ± 1.00	1.77 ± 0.25	1.70 ± 0.58	3.32
Ni	13.5 ± 2.1	7.08 ± 0.83	8.62 ± 1.29	15.5
Cu	11.9 ± 1.5	8.66 ± 1.42	9.62 ± 1.83	39.4
Zn	31.2 ± 3.9	20.1 ± 2.6	24.6 ± 6.0	37.3
Ga	12.7 ± 1.3	14.1 ± 1.6	14.3 ± 0.9	22.0
As	5.32 ± 0.65	3.82 ± 0.81	5.63 ± 1.1	4.08
Rb	94.0 ± 9.9	113 ± 15	111 ± 7	82.7
Sr	70.7 ± 19.1	141 ± 16	130 ± 23	63.3
Y	24.1 ± 1.6	28.3 ± 3.2	22.2 ± 1.6	12.7
Zr	329 ± 25	387 ± 67	299 ± 18	202
Nb	20.8 ± 0.7	19.2 ± 1.0	19.2 ± 0.6	18.3

Appendix B (*continued*)

Elements	CDCL (n = 9; ±σ)	ETPL (n = 11; ±σ)	LPQL (n = 5; ±σ)	Weathered red sandstone
Sn	2.76 ± 0.18	2.99 ± 0.30	3.29 ± 1.16	1.97
Cs	9.78 ± 1.46	7.42 ± 1.84	7.93 ± 1.13	6.93
Ba	316 ± 62	482 ± 67	489 ± 36	407
La	28.2 ± 1.9	40.0 ± 5.3	28.5 ± 1.0	10.6
Ce	55.2 ± 3.7	79.3 ± 10.4	56.1 ± 1.9	19.2
Pr	6.09 ± 0.43	8.86 ± 1.17	6.26 ± 0.24	1.95
Nd	22.2 ± 1.5	32.6 ± 4.2	23.1 ± 0.9	6.84
Sm	3.68 ± 0.31	5.6 ± 0.62	4.13 ± 0.26	1.23
Eu	0.686 ± 0.058	1.04 ± 0.09	0.813 ± 0.061	0.31
Gd	3.39 ± 0.28	4.83 ± 047	3.62 ± 0.31	1.29
Tb	0.568 ± 0.045	0.741 ± 0.069	0.564 ± 0.039	0.24
Dy	3.77 ± 0.26	4.63 ± 0.50	3.58 ± 0.26	1.85
Ho	0.811 ± 0.060	0.955 ± 0.106	0.754 ± 0.059	0.43
Er	2.52 ± 0.17	2.90 ± 0.31	2.33 ± 0.16	1.40
Tm	0.388 ± 0.025	0.436 ± 0.044	0.356 ± 0.025	0.22
Yb	2.70 ± 0.17	3.00 ± 0.31	2.49 ± 0.15	1.61
Lu	0.408 ± 0.024	0.450 ± 0.047	0.376 ± 0.018	0.25
Hf	8.69 ± 0.60	10.1 ± 1.8	7.76 ± 0.46	4.96
Ta	1.81 ± 0.11	1.68 ± 0.09	1.60 ± 0.03	1.36
Tl	0.555 ± 0.048	0.550 ± 0.064	0.541 ± 0.026	0.45
Pb	6.05 ± 0.78	8.05 ± 0.65	7.76 ± 0.43	13.3
Bi	0.093 ± 0.016	0.061 ± 0.010	0.073 ± 0.012	0.07
Th	8.61 ± 0.53	12.3 ± 1.0	8.45 ± 0.50	4.14
U	2.83 ± 0.14	3.15 ± 0.26	2.61 ± 0.08	1.53

Appendix C

Sm and Nd concentrations and isotopic data by grain size fraction in the Chengdu Clay and the adjacent loess.

Sample	Sm (μg/g)	Nd (μg/g)	$^{147}Sm/^{144}Nd$	$^{143}Nd/^{144}Nd$ (±2σ)	$f^{Sm/Nd}$ [a]	$\varepsilon_{Nd}(0)$ [b]	T_{Nd} [c] (Ga)
Loess on the Chinese Loess Plateau (*LT-25*) [d]							
<2 μm	2.66	15.87	0.1012	0.512017 ± 0.000013	−0.485	−12.11	1.53
2–5 μm	3.43	19.67	0.1056	0.512045 ± 0.000013	−0.463	−11.56	1.55
5–10 μm	3.43	19.36	0.1073	0.512050 ± 0.000014	−0.455	−11.48	1.57
10–20 μm	3.86	21.24	0.1097	0.512047 ± 0.000014	−0.442	−11.52	1.61
20–32 μm	4.02	21.60	0.1126	0.512042 ± 0.000013	−0.428	−11.62	1.67
32–50 μm	4.15	22.18	0.1131	0.512068 ± 0.000013	−0.425	−11.12	1.64
>50 μm	5.05	26.63	0.1146	0.512078 ± 0.000014	−0.417	−10.93	1.65
WS[e]	3.69	20.40	0.1093	0.512077 ± 0.000011	−0.444	−10.95	1.56
Chengdu Clay (*JTW1-3*)							
<2 μm	1.56	12.60	0.0745	0.512135 ± 0.000029[f]	−0.621	−9.81	1.11
2–5 μm	2.55	21.60	0.0712	0.512221 ± 0.000021	−0.638	−8.13	0.99
5–10 μm	3.05	25.00	0.0738	0.511998 ± 0.000007	−0.625	−12.48	1.25
10–20 μm	2.70	22.30	0.0731	0.512025 ± 0.000009	−0.628	−11.96	1.22
20–32 μm	2.71	19.70	0.0834	0.511997 ± 0.000008	−0.576	−12.50	1.35
32–50 μm	2.29	18.20	0.0763	0.512042 ± 0.000013	−0.612	−11.63	1.23
>50 μm	0.84	6.49	0.0784	0.511900 ± 0.000007	−0.601	−14.40	1.41
WS[e]	1.90	15.40	0.0747	0.511972 ± 0.000014	−0.620	−12.99	1.29
Loess on the eastern Tibetan Plateau (*GZ1-2*)							
<2 μm	2.78	22.20	0.0759	0.511909 ± 0.000014	−0.614	−14.22	1.37
2–5 μm	3.42	27.60	0.0748	0.511982 ± 0.000009	−0.620	−12.80	1.28
5–10 μm	2.85	21.20	0.0810	0.512002 ± 0.000006	−0.588	−12.41	1.32
10–20 μm	3.63	29.30	0.0747	0.512031 ± 0.000007	−0.620	−11.84	1.23
20–32 μm	3.38	25.60	0.0798	0.512032 ± 0.000006	−0.594	−11.82	1.27
32–50 μm	3.24	24.30	0.0806	0.512004 ± 0.000006	−0.590	−12.37	1.31
>50 μm	4.17	33.00	0.0762	0.512005 ± 0.000006	−0.613	−12.35	1.27
WS[e]	3.91	29.80	0.0794	0.511970 ± 0.000006	−0.596	−13.03	1.34

[a] The $f^{Sm/Nd}$ notation describes deviation of $^{147}Sm/^{144}Nd$ from a chondritic uniform reservoir (CHUR). $f^{Sm/Nd} = [(^{147}Sm/^{144}Nd)_{Sample}/(^{147}Sm/^{144}Nd)_{CHUR} - 1]$, where $(^{147}Sm/^{144}Nd)_{CHUR} = 0.1967$.

[b] The $\varepsilon_{Nd}(0)$ notation describes deviation of $^{143}Nd/^{144}Nd$ (in part per 10^4) from a CHUR reservoir. $\varepsilon_{Nd}(0) = (^{143}Nd/^{144}Nd)_{Sample}/(^{143}Nd/^{144}Nd)_{CHUR} - 1] \times 10^4$, where $(^{143}Nd/^{144}Nd)_{CHUR} = 0.512638$.

[c] The T_{Nd} is the Sm–Nd crustal residence age calculated relative to depleted mantle (DM) reservoir. $T_{Nd} = (1/\lambda_{Sm})\ln[((^{143}Nd/^{144}Nd)_{Sample} - (^{143}Nd/^{144}Nd)_{DM})/((^{147}Sm/^{144}Nd)_{Sample} - (^{147}Sm/^{144}Nd)_{DM}) + 1]$, where $(^{143}Nd/^{144}Nd)_{DM} = 0.51315$, $(^{147}Sm/^{144}Nd)_{DM} = 0.2137$, $\lambda_{Sm} = 6.54 \times 10^{-12}$ yr^{-1}.

[d] Data of loess on the Chinese Loess Plateau (LT-25) after Feng et al. (2009).

[e] WS–Whole silicate mineral sample.

[f] Data of $^{143}Nd/^{144}Nd$ for Chengdu Clay (JTW1-3) and loess on the eastern Tibetan Plateau (GZ1-2) after Feng et al. (2010).

References

Anders, E., Grevesse, N., 1989. Abundances of the elements: meteoritic and solar. Geochim. Cosmochim. Acta 53, 197–214.

Blott, S.J., Pye, K., 2001. Gradistat: a grain size distribution and statistics package for the analysis of unconsolidated sediments. Earth Surf. Proc. Land. 26, 1237–1248.

Chen, Z.R., He, Y.W., 1990. A preliminary discussion on date determination of Guanghan clay and Chengdu Clay with ^{14}C dates. Mt. Res. 8, 167–173 (in Chinese).

Chen, C.-T.A., Lan, H.-C., Lou, J.-Y., Chen, Y.-C., 2003. The dry Holocene megathermal in Inner Mongolia. Palaeogeogr. Palaeoclimatol. Palaeoecol. 193, 181–200.

Chu, L.T., 1937. A reconnaissance soil survey of Chengtu area, Szechuan. Soil Bull. 18, 1–70.

Clarke, M.L., 1995. Sedimentological characteristics and rare earth element fingerprinting of Tibetan silts and their relationship with sediments of the western Chinese Loess Plateau. Quat. Proc. 4, 41–51.

Clayton, R.N., Mayeda, T.K., 1963. The use of bromine pentafluoride in the extraction of oxygen from oxides and silicates for isotopic analysis. Geochim. Cosmochim. Acta 27, 43–52.

Clayton, R.N., Rex, R.W., Syers, J.K., Jackson, M.L., 1972. Oxygen isotope abundance in quartz from Pacific pelagic sediments. J. Geophys. Res. 77, 3907–3915.

Clayton, R.N., Jackson, M.L., Sridhar, K., 1978. Resistance of quartz silt to isotopic exchange under burial intense weathering conditions. Geochim. Cosmochim. Acta 42, 1517–1522.

Cullers, R.L., Basu, A., Suttner, L., 1988. Geochemical signature of provenance in sand-size material in soils and stream sediments near the Tobacco Root batholith, Montana, USA. Chem. Geol. 70, 335–348.

Derbyshire, E., Meng, X.M., Kemp, R.A., 1997. Climate change, loess and palaeosols: proxy measures and resolution in North China. J. Geol. Soc. (Lond.) 154, 793–805.

Derbyshire, E., Meng, X.M., Kemp, R.A., 1998. Provenance, transport and characteristics of modern eolian dust in western Gansu Province, China, and interpretation of the Quaternary loess record. J. Arid Environ. 39, 497–516.

Fang, X., 1995. The origin and provenance of the Malan loess along the eastern margin of the Qinghai–Xizang (Tibetan) Plateau and its adjacent area. Sci. China Ser. B 38, 876–887.

Fang, X., Han, Y., Ma, J., Song, L., Yang, S., Zhang, X., 2004. Dust storms and loess accumulation on the Tibetan Plateau: a case study of dust event on 4 March 2003 in Lhasa. Chin. Sci. Bull. 49, 953–960.

Feng, J.-L., Zhu, L.-P., Ju, J.-T., Zhou, L.-P., Zhen, X.-L., Zhang, W., Gao, S.-P., 2008. Heavy dust fall in Beijing, on April 16–17, 2006: geochemical properties and indications of the dust provenance. Geochem. J. 42, 221–236.

Feng, J.-L., Zhu, L.-P., Zhen, X.-L., Hu, Z.-G., 2009. Grain size effect on Sr and Nd isotopic compositions in eolian dust: implications for tracing dust provenance and Nd model age. Geochem. J. 43, 123–131.

Feng, J.-L., Hu, Z.-G., Cui, J.-Y., Zhu, L.-P., 2010. Distributions of lead isotopes with grain size in aeolian deposits. Terra Nova 22, 257–263.

Feng, J.-L., Hu, Z.-G., Ju, J.-T., Zhu, L.-P., 2011. Variations in trace element (including rare earth element) concentrations with grain sizes in loess and their implications for tracing the provenance of eolian deposits. Quat. Int. 236, 116–126.

Goldstein, S.L., 1988. Decoupled evolution of Nd and Sr isotopes in the continental crust and the mantle. Nature 336, 733–738.

Götze, J., Zimmerle, W., 2000. Quartz and silica as guide to provenance in sediments and sedimentary rocks. In: Aigner, T., Cross, T., Wright, V.P. (Eds.), Contributions to Sedimentary Geology. Schweizerbart'sche, Stuttgart, pp. 10–46.

Gu, Z.Y., Liu, T.S., Zheng, S.H., 1987. A preliminary study on quartz oxygen isotope in Chinese loess and soils. In: Liu, T.S. (Ed.), Aspects of Loess Research. China Ocean Press, Beijing, pp. 291–301.

Han, Y., Fang, X., Kang, S., Wang, H., Kang, F., 2008. Shifts of dust source regions over central Asia and the Tibetan Plateau: connections with the Arctic oscillation and the westerly jet. Atmos. Environ. 42, 2358–2368.

Han, W., Fang, X., Yang, S., King, J., 2010. Differences between East Asian and Indian monsoon climate records during MIS3 attributed to differences in their driving mechanisms: evidence from the loess record in the Sichuan basin, southwestern China and other continental and marine climate records. Quat. Int. 218, 94–103.

Hao, Q., Guo, Z., Qiao, Y., Xu, B., Oldfield, F., 2010. Geochemical evidence for the provenance of middle Pleistocene loess deposits in southern China. Quat. Sci. Rev. 29, 3317–3326.

Harland, W.B., 1945. On the physiographical history of Western Szechuan with special reference to the ice age in the red basin. J. W. China Border Res. Soc. (Chengtu) Ser. B. 15, 1–19.

Heller, F., Liu, T.S., 1982. Magnetostratigraphical dating of loess deposits in China. Nature 300, 431–433.

Hesse, P.P., McTainsh, G.H., 1999. Last Glacial Maximum to early Holocene wind strength in the mid-latitudes of the southern hemisphere from aeolian dust in the Tasman Sea. Quat. Res. 52, 343–349.

Hou, S.S., Yang, S.L., Sun, J.M., Ding, Z.L., 2003. Oxygen isotope compositions of quartz grains (4–16 μm) from Chinese aeolian deposits and their implications for provenance. Sci. China Ser. D 46, 1003–1011.

Hseung, Y., 1944. Properties and genesis of Pleistocene clay in the Jiangxi Province. Geol. Rev. 9, 109–120 (in Chinese).

Hu, Z.-G., Feng, J.-L., Ju, J.-T., 2010. Grain size distribution and micro-structure of quartz in the Chengdu Clay. J. Mt. Sci. 28, 392–406 (in Chinese, with English Abstr.).

Jackson, M.L., Sayin, M., Clayton, R.N., 1976. Hexafluorosilicic acid reagent modification for quartz isolation. Soil Sci. Soc. Am. J. 40 (958–910).

Kapp, P., Pelletier, J.D., Rohrmann, A., Heermance, R., Russell, J., Ding, L., 2011. Wind erosion in the Qaidam basin, central Asia: implications for tectonics, paleoclimate, and the source of the Loess Plateau. GSA Today 21, 4–10.

Kirby, E., Reiners, P.W., Krol, M.A., Whipple, K.X., Hodges, K.V., Farley, K.A., Tang, W., Chen, Z., 2002. Late Cenozoic evolution of the eastern margin of the Tibetan Plateau: inferences from $^{40}Ar/^{39}Ar$ and (U–Th)/He thermochronology. Tectonics 21. http://dx.doi.org/10.1029/2000TC001246.

Kong, D.F., 1994. Fractured Clay. Geological Publishing House, Beijing (in Chinese).

Kukla, G., Heller, F., Liu, X.M., Chun, X.T., Liu, T.S., An, Z.S., 1988. Pleistocene climates in China dated by magnetic susceptibility. Geology 16, 811–814.

Lehmkuhl, F., Klinge, M., Rees-Jones, J., Rhodes, E.J., 2000. Late Quaternary eolian sedimentation in central and south-eastern Tibet. Quat. Int. 68/71, 117–132.

Li, C.-Y., 1947. Genesis of gravel horizon during Ya'an and Jiangbei Period. Geol. Rev. 12, 17–126.

Li, C.-S., Wu, Y.-S., Li, Y.-Z., Lu, D.-S., 1964. Relicts of Quarternary glacier in the southern Longmen Mountains, Sichuan. In: Quarternary Committee, Chinese (Ed.), Corpus on the Quaternary Glacier Relicts in China. Science Press, Beijing, pp. 14–84.

Liu, X.S., 1983. Quaternary in the Sichuan Basin. Sichuan Sci. Technol. Pre., Chengdu (in Chinese).

Liu, T.S., 1985. Loess and the Environment. China Ocean Press, Beijing.

Liu, T.S., Chang, T.H., 1964. The 'Huangtu' (loess) of China. Rept. 6th INQUA Congress Warsaw 1961, 4, pp. 503–524.

Lu, Y.C., Wen, Q.Z., Huang, B.J., Min, Y.S., Deng, H.X., 1976. A preliminary discussion on the source of loessic materials in China — a study of the surface textures of silt quartz grains by transmission electron microscope. Geochimica 1, 47–53 (in Chinese).

Lu, H., Wang, X., Ma, H., Tan, H., Vandenberghe, J., Miao, X., Li, Z., Sun, Y., An, Z., Cao, G., 2004. The Plateau Monsoon variation during the past 130 kyr revealed by loess deposit at northeast Qinghai–Tibet (China). Global Planet. Chang. 41, 207–214.

Lü, L., Fang, X., Lu, H., Han, Y., Yang, S., Li, J., An, Z., 2004. Millennial-scale climate change since the last glaciation recorded by grain sizes of loess deposits on the northeastern Tibetan Plateau. Chin. Sci. Bull. 49, 1157–1164.

Ma, R.Z., 1944. Formation of Chinese loess. Geol. Rev. 9, 205–224 (in Chinese).

Maher, B.A., Prospero, J.M., Mackie, D., Gaiero, D., Hesse, P.P., Balkanski, Y., 2010. Global connections between aeolian dust, climate and ocean biogeochemistry at the present day and at the last glacial maximum. Earth-Sci. Rev. 99, 61–97.

Miao, X., Sun, Y., Lu, H., Mason, J.A., 2004. Spatial pattern of grain size in the Late Pliocene 'Red Clay' deposits (North China) indicates transport by low-level northerly winds. Palaeogeogr. Palaeoclimatol. Palaeoecol. 206, 149–155.

Moreno, P.I., León, A.L., 2003. Abrupt vegetation changes during the last glacial to Holocene transition in mid-latitude South America. J. Quat. Sci. 18, 787–800.

Moreno, A., Cacho, I., Canals, M., Prins, M.A., Sanchez-Goni, M.F., Grimalt, J.O., Weltje, G.J., 2002. Saharan dust transport and high-latitude glacial climate variability: the Alboran Sea record. Quat. Res. 58, 318–328.

Muhs, D.R., Bettis III, E.A., 2000. Geochemical variations in Peoria Loess of Western Iowa indicate paleowinds of Midcontinental North America during last glaciation. Quat. Res. 53, 49–61.

Muhs, D.R., Budahn, J.R., 2006. Geochemical evidence for the origin of late Quaternary loess in central Alaska. Can. J. Earth Sci. 43, 323–337.

Muhs, D.R., Budahn, J.R., Johnson, D.L., Reheis, M., Beann, J., Skipp, G., Fisher, E., Jones, J.A., 2008. Geochemical evidence for airborne dust additions to soils in Channel Islands National Park, California. Bull. Geol. Soc. Am. 120, 106–126.

Nagashima, K., Tada, R., Matsui, H., Irino, T., Tani, A., Toyoda, S., 2007. Orbital- and millennial-scale variations in Asian dust transport path to the Japan Sea. Palaeogeogr. Palaeoclimatol. Palaeoecol. 247, 144–161.

Nagashima, K., Tada, R., Tani, A., Sun, Y., Isozaki, Y., Toyoda, S., Hasegawa, H., 2011. Millennial-scale oscillations of the westerly jet path during the last glacial period. J. Asian Earth Sci. 40, 1214–1220.

Ono, Y., Irino, T., 2004. Southern migration of westerlies in the Northern Hemisphere PEP II transect during the Last Glacial Maximum. Quat. Int. 118/119, 13–22.

Ouimet, W.B., Whipple, K.X., Royden, L.R., Sun, Z., Chen, Z., 2007. The influence of large landslides on river incision in a transient landscape: Eastern margin of the Tibetan Plateau (Sichuan, China). Geol. Soc. Am. Bull. 119, 1462–1476.

Porter, S.C., An, Z., 1995. Correlation between climate events in the North Atlantic and China during the last glaciation. Nature 375, 305–308.

Pye, K.A., 1987. Aeolian Dust and Dust Deposit. Academic Press, London.

Pye, K., Zhou, L.P., 1989. Late Pleistocene and Holocene aeolian dust deposition in North China and the Northwest Pacific Ocean. Palaeogeogr. Palaeoclimatol. Palaeoecol. 73, 11–23.

Qi, L., Hu, J., Gregoire, D.C., 2000. Determination of trace elements in granites by inductively coupled plasma mass spectrometry. Talanta 51, 507–513.

Qiao, Y., Zhao, Z., Li, Z., Wang, Y., Fu, J., Wang, S., Li, C., Yao, H., Jiang, F., 2007. Aeolian origin of the red earth formation in the Chengdu Plain. Quat. Sci. 27, 286–294 (in Chinese, with English Abstr.).

Rea, D.K., 1994. The paleoclimatic record provided by eolian deposition in the deep sea: the geologic history of wind. Rev. Geophys. 32, 159–195.

Rea, D.K., Leinen, M., 1988. Asian aridity and the zonal westerlies: Late Pleistocene and Holocene record of eolian deposition in the northwest Pacific Ocean. Palaeogeogr. Palaeoclimatol. Palaeoecol. 66, 1–8.

Rex, R.W., Syers, J.K., Jackson, M.L., Clayton, R.N., 1969. Eolian origin of quartz in soils of Hawaii islands and in Pacific Pelagic sediments. Science 163, 277–279.

Richardson, H.L., 1942. Soils and agriculture of Szechwan. National Agriculture Research Bureau, Special Publication No. 27. Ministry Agriculture and Forestry, Chungking.

Richardson, H.L., 1943. The ice age in west China. J. W. China Border Res. Soc. (Chengtu) Ser. B 14, 1–27.

Salfeld, H., 1936. Über die diluviale vereisung von West-Szechuan (China) und insbesonders der Chengtu-Ebene. Zbl. Mineral. Geol. Paläontol. Abt. B (9), 353–357.

Schaetzl, R.J., Attig, J.W., 2013. The loess cover of northeastern Wisconsin. Quat. Res. 79, 199–214.

Schiemann, R., Luthi, D., Schar, C., 2009. Seasonality and interannual variability of the Westerly Jet in the Tibetan Plateau region. J. Clim. 22, 2940–2957.
Shao, Z.G., Li, D.J., Li, Y.Z., 1984. Geological features of Pleistocene clay in the Chengdu plain. In: Geological Society of China (Ed.), Corpus on the Quaternary Glacier and Quaternary. Geological Press, Beijing, pp. 142–153 (in Chinese).
Stuut, J.-B., Smalley, I., O'Hara-Dhand, K., 2009. Aeolian dust in Europe: African sources and European deposits. Quat. Int. 198, 234–245.
Sun, J.M., Li, S.H., Muhs, D.R., Li, B., 2007a. Loess sedimentation in Tibet: provenance, processes, and link with Quaternary glaciations. Quat. Sci. Rev. 26, 2265–2280.
Sun, Y.B., Clemens, S.C., An, Z.S., Yu, Z.W., 2006. Astronomical timescale and palaeoclimatic implication of stacked 3.6-Myr monsoon records from the Chinese Loess Plateau. Quat. Sci. Rev. 25, 33–48.
Sun, Y.B., Tada, R., Chen, J., Chen, H.Z., Toyoda, S., Tani, A., Isozaki, Y., Nagashima, K., Hasegawa, H., Ji, J.F., 2007b. Distinguishing the sources of Asian dust based on electron spin resonance signal intensity and crystallinity of quartz. Atmos. Environ. 41, 8537–8548.
Sun, Y.B., Tada, R., Chen, J., Liu, Q.S., Toyoda, S., Tani, A., Ji, J.F., Isozaki, Y., 2008. Tracing the provenance of fine-grained dust deposited on the central Chinese Loess Plateau. Geophys. Res. Lett. 35. http://dx.doi.org/10.1029/2007GL031672 (L01804).
Tang, M.C., 1998. Formation, evolution and the oscillation of the Tibetan Plateau monsoon. Gansu Meteorol. 16, 1–14 (in Chinese).
Tang, M.C., Reiter, E.R., 1984. Plateau monsoons of the Northern Hemisphere: a comparison between North America and Tibet. Mon. Weather Rev. 112, 617–637.
Taylor, S.R., McLennan, S.M., 1985. The Continental Crust: Its Composition and Evolution. Blackwell Scientific Publications, London.
Taylor, S.R., McLennan, S.M., McCulloch, M.T., 1983. Geochemistry of loess, continental crustal composition and crustal model ages. Geochim. Cosmochim. Acta 47, 1897–1905.
Thorp, J., 1939. Geography of the Soils of China. The National Geological Survey of China, Beijing.
Thorp, J., Dye, D.S., 1936. The Chengtu Clays—deposits of possible loessial origin in western and northwestern Szechuan Basin. Bull. Geol. Soc. China 15, 225–246.
Thorson, R.M., Bender, G., 1985. Eolian deflation by ancient katabatic winds: a late Quaternary example from the north Alaska Range. Bull. Geol. Soc. Am. 96, 702–709.
Toggweiler, J.R., Russell, J., 2008. Ocean circulation in a warming climate. Nature 451, 286–288.
Tsoar, H., Pye, K.A., 1987. Dust transport and question of desert loess formation. Sedimentology 34, 139–153.
Wang, W.G., 1998. The summary history of landforms evolution in Mianyang. J. Southwest China Inst. Technol. 13, 72–76 (in Chinese, with English Abstr.).
Wang, B., Nie, Q.Y., Wang, Y.S., Zhang, J.Y., 2002. Discussion on the genetic mechanism of the Chengdu Clay. J. Geol. Hazards Environ. Preserv. 13, 54–56 (in Chinese, with English Abstr.).
Williams, G.P., Bryan, K., 2006. Ice Age winds: an aquaplanet model. J. Clim. 19, 1706–1715.
Xiao, J.L., Porter, S.C., An, Z.S., Kumai, H., Yoshikawa, S., 1995. Grain size of Quartz as an indicator of winter monsoon strength on the Loess Plateau of central China during the last 130,000 yr. Quart. Res. 43, 22–29.
Xiao, J.L., Inouchi, Y., Kumai, H., Yoshikawa, S., Kondo, Y., Liu, T., An, Z., 1997. Eolian quartz flux to Lake Biwa, Central Japan, over the past 145,000 years. Quart. Res. 48, 48–57.
Xu, S., Gao, Y., 1962. Monsoon phenomenon on the Tibetan Plateau. Acta Geograph. Sin. 28, 111–123 (in Chinese, with Russian Abstr.).
Yang, S., Fang, X., Shi, Z., Lehmkuhl, F., Song, C., Han, Y., Han, W., 2010a. Timing and provenance of loess in the Sichuan Basin, southwestern China. Palaeogeogr. Palaeoclimatol. Palaeoecol. 292, 144–154.
Yang, S., Fang, X., Yan, M., Shi, Z., Song, C., Han, Y., 2010b. Grain size profiles in the Chengdu Clay, eastern margin of the Tibetan Plateau: implications for significant drying of Asia since 500 ka B.P. J. Asian Earth Sci. 38, 57–64.
Yin, J.H., 2005. A consistent poleward shift of the storm tracks in simulations of 21st century climate. Geophys. Res. Lett. 32. http://dx.doi.org/10.1029/2005GL023684 L18701.
Yokoo, Y., Nakano, T., Nishikawa, M., Hao, Q., 2004. Mineralogical variation of Sr–Nd isotopic and elemental compositions in loess and desert sand from the central Loess Plateau in China as a provenance tracer of wet and dry deposition in the northwestern Pacific. Chem. Geol. 204, 45–62.
Young, C.C., 1937. New Triassic and Cretaceous Reptiles in China. Bull. Geol. Soc. China 17, 109–120.
Yü, H., 1940. Soils of Kwansyu, Chaohua, and Chienke. Soils Quart. 1, 1–10 (in Chinese).
Zhang, H.-Y., 1988. Genesis of the Chengdu Clay based on micro-fracture research. Hydrogeol. Eng. Geol. (1), 17–19 (in Chinese).
Zhang, X., Shen, Z., Zhang, G., Chen, T., Liu, H., 1996. Remote mineral aerosol in westerlies and their contributions to the Chinese Loess. Sci. China Ser. D. 39, 134–143.
Zhang, X., Arimoto, R., Cao, J., An, Z., Wang, D., 2001. Atmospheric dust aerosol over the Tibetan Plateau. J. Geophys. Res. 106, 18471–18476.
Zhao, Z., Qiao, Y., Wang, Y., Fu, J., Wang, S., Li, C., Yao, H., Jiang, F., 2007. Magnetostratigraphic and paleoclimatic studies on the red earth formation from the Chengdu Plain in Sichuan Province. China. Sci. China Ser. D 50, 927–935.
Zhou, X.-L., 1986. Calcarious concretions in the Chengdu Clay. Hydrogeol. Eng. Geol. (4), 29–31 (in Chinese).